Structure-Function Relationships in Perimetric Glaucoma: Comparison of Minimum-Rim Width and Retinal Nerve Fiber Layer Parameters

Navid Amini,[1] Ramin Daneshvar,[1,2] Farideh Sharifipour,[1,3] Pablo Romero,[1,4] Sharon Henry,[1] Joseph Caprioli,[1] and Kouros Nouri-Mahdavi[1]

[1]Glaucoma Division, Stein Eye Institute, David Geffen School of Medicine, University of California Los Angeles, Los Angeles, California, United States
[2]Eye Research Center, Mashhad University of Medical Sciences, Mashhad, Iran
[3]Department of Ophthalmology, Ahvaz Jundishapur University of Medical Sciences, Ahvaz, Iran
[4]Department of Ophthalmology, University of Chile, Santiago, Chile

Correspondence: Kouros Nouri-Mahdavi, Stein Eye Institute, 100 Stein Plaza, Los Angeles, CA 90095, USA;
nouri-mahdavi@jsei.ucla.edu.

NA and RD contributed equally to the work presented here and should therefore be regarded as equivalent first authors.

Submitted: March 25, 2017
Accepted: August 2, 2017

Citation: Amini N, Daneshvar R, Sharifipour F, et al. Structure-function relationships in perimetric glaucoma: comparison of minimum-rim width and retinal nerve fiber layer parameters. *Invest Ophthalmol Vis Sci*. 2017;58:4623–4631. DOI:10.1167/iovs.17-21936

Purpose. To test the hypotheses that: (1) structure–function (SF) relationships between visual fields (VF) and Bruch's membrane opening-based minimum rim width (BMO-MRW) measurements are superior to those for peripapillary retinal nerve fiber layer (pRNFL) in perimetric glaucoma; (2) BMO-MRW measurements may extend the utility of structural measurement across the range of glaucoma severity; and (3) to estimate the influence of Bruch's membrane opening (BMO) size on BMO-MRW measurements.

Methods. One hundred eight perimetric glaucoma eyes (68 patients) with good quality spectral-domain optical coherence tomography images of the optic disc and pRNFL, and reliable VF within 6 months were recruited. Relationship of global and sectoral BMO-MRW and pRNFL thickness with corresponding VF parameters and the influence of normalizing BMO-MRW (on BMO circumference, nBMO-MRW) on SF relationships were investigated. Broken-stick models were used to compare the point at which pRNFL and BMO-MRW parameters reached their measurement floor.

Results. The median (interquartile range) of VF mean deviation was −5.9 (−12.6 to −3.6) dB. Spearman correlation coefficients between pRNFL, BMO-MRW, and nBMO-MRW measures and corresponding VF cluster average deviations ranged between 0.55 to 0.80, 0.35 to 0.66, and 0.38 to 0.65, respectively. Bruch's membrane opening–MRW parameters demonstrated weaker SF relationships compared with pRNFL globally and in temporal, temporal-superior, and nasal-inferior sectors ($P < 0.03$). Normalization of BMO-MRW did not significantly influence SF relationships.

Conclusions. Structure–function relationships were somewhat weaker with BMO-MRW parameters compared with pRNFL in eyes with perimetric glaucoma. Bruch's membrane opening–MRW normalization did not significantly change SF relationships in this group of eyes with mild departures from average BMO size.

Keywords: glaucoma, optical coherence tomography, BMO-MRW, RNFL

Glaucoma is a progressive optic neuropathy characterized by retinal ganglion cell loss. This cell loss is manifest by structural changes in the optic nerve head (ONH) and retinal nerve fiber layer (RNFL) with associated functional deficits. While the peripapillary RNFL (pRNFL) thickness has been traditionally used for detection of early glaucoma with optical coherence tomography (OCT), more recently, minimum rim width measurement estimated from the Bruch membrane opening (BMO-MRW) has been proposed as a valid alternative structural measure.[1] The BMO-MRW is defined as the minimum distance between the internal limiting membrane (ILM) on the surface of ganglion cell axons as they enter the optic disc and the termination of Bruch membrane, known as the BMO.[2] This parameter is independent of any arbitrary reference planes and is geometrically more precise than 'cup' or 'rim' measurement based on an operator-defined 'contour line' around the visible disc margin.[2,3] There is controversy whether BMO-MRW is superior to pRNFL for detection of early glaucoma or with regard to structure–function (SF) relationships.[1,2,4] One caveat is that the BMO-MRW measurements can vary as a function of BMO size: eyes with a smaller disc size would be expected to have thicker BMO-MRW measurements compared with eyes with a larger disc size given the same number of ganglion cell axons.[5] The magnitude of this confounding issue has not been well explored, although a new parameter, minimum rim area (i.e., the area through which the axons would pass to enter the optic nerve) has been proposed to address this issue.[6]

One shortcoming of global structural measures, such as pRNFL thickness, BMO-MRW, or macular parameters is that they tend to reach their measurement floor as the visual field (VF) mean deviation (MD) demonstrates a depression of approximately 1 log unit (approximately −10 dB of total

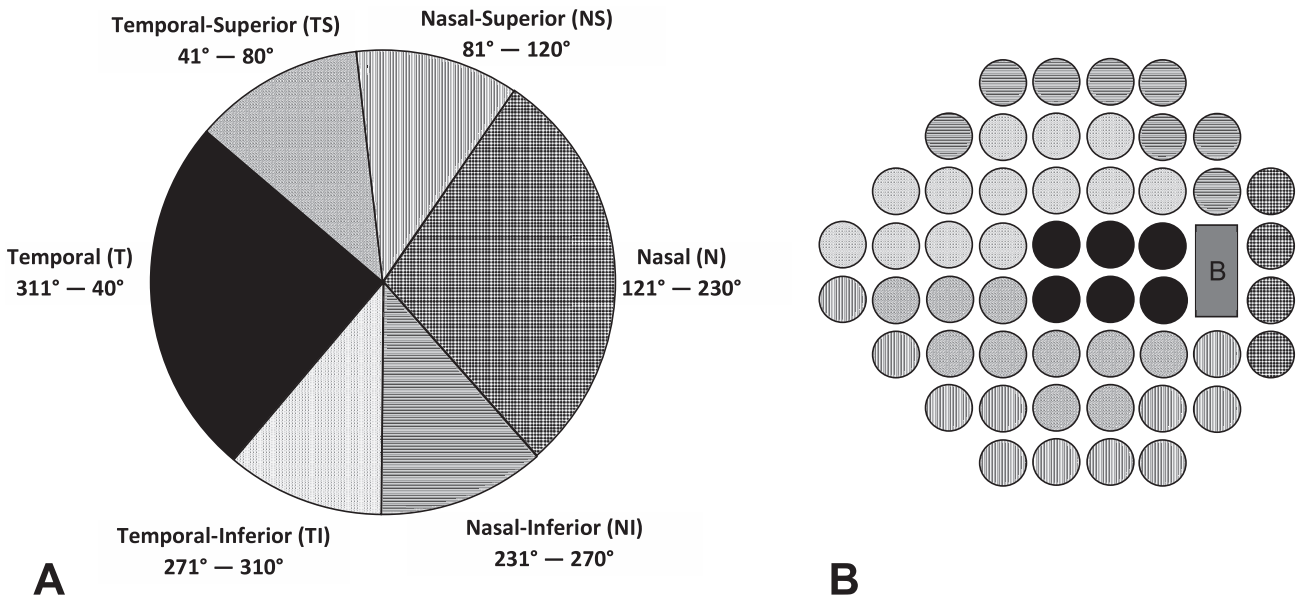

FIGURE 1. Garway-Heath and colleagues'[9,10] model for the correlation between ONH sectors (**A**) and VF clusters (**B**). Letter 'B' in the right hand side image represents the test locations corresponding to the blind spot, which were excluded.

deviation).[7] This residual thickness (at measurement floor) is attributed to nonneural tissues, such as blood vessels and glial cells.[7] However, clinically, neuroretinal rim loss is frequently observed to be total with no neural or nonneural tissue remaining where notching or rim loss extends to what clinically is known to be the scleral rim as seen on examination or stereoscopic disc photographs. This raises the question of whether the BMO-MRW measurements could reach a lower floor of measurement later than pRNFL during the course of the disease, and hence, BMO-MRW measurements might be more useful in more advanced stages of the disease. Another important factor to consider in this context is the dynamic range of any given parameter (i.e., not only is it important when the floor is reached, but one has also to consider the rate of change of the parameter down to the final floor).

The purpose of the present study is to test the hypotheses that: (1) SF relationships are stronger with BMO-MRW measurements compared with pRNFL in perimetric glaucoma patients; (2) BMO-MRW measurements need to be corrected for the BMO size to optimally reflect SF relationships; and (3) using BMO-MRW extend the useful range of structural measurements in glaucoma.

METHODS

Participants

Patients meeting the inclusion criteria were selected from multiple ongoing studies at the Stein Eye Institute. Patients with established glaucoma with best-corrected visual acuity of 20/80 or better, spherical refractive error between −7 and +3 diopters (D), and reliable VF and OCT exams within 6 months of each other were included. Exclusion criteria consisted of inability to provide reliable, reproducible VFs, cylindrical error more than 3 D, significant retinal disease, nonglaucomatous optic neuropathy, and anomalous optic discs. Approval of the institutional review board at the University of California, Los Angeles was obtained prior to conduct of the study and the study adhered to the tenets of the Declaration of Helsinki and Health Insurance Portability and Accountability Act.

Study eyes underwent a thorough eye exam, including best-corrected visual acuity, refraction, corneal pachymetry, slit-lamp examination, IOP measurement with Goldmann applanation tonometry, gonioscopy, dilated fundus examination, biometry with IOLMaster (Carl Zeiss Meditec, Dublin, CA, USA), and achromatic VF testing (Swedish Interactive Thresholding Algorithm [SITA]-Standard 24-2 fields; Humphrey Field Analyzer, Carl Zeiss Meditec). Glaucoma was defined as the presence of glaucomatous optic nerve damage based on apparent rim parameters (i.e., vertical cup-to-disc ratio of >0.6, cup to disc asymmetry >0.2, or presence of focal rim thinning or notching) along with a corresponding VF defect on perimetry. A VF defect was considered to be present on 24-2 fields if both of the following criteria were met: (1) glaucoma hemifield test outside normal limits, and (2) four abnormal points with *P* less than 5% on the pattern deviation plot, both confirmed at least once.[8]

Visual Field and Imaging Methods

All subjects had reliable VFs with confirmed reproducible VF loss as described above. Reliable VFs were defined as fixation loss and false-negative rates less than 25% and a false-positive rate less than 15%. Test points were grouped into six sectors corresponding to optic disc regions based on clinically defined disc margin, as described by Garway-Heath and colleagues (Fig. 1).[9,10] The two points immediately above and below the physiologic blind spot were excluded from the analysis and the remaining 52 points were used to calculate the average deviation (AD) in each sector based on the total deviation numerical plot. To calculate the AD in each sector, defect depth in decibel units was first converted to a linear scale (1/Lambert) for each test point and then averaged and converted back to the logarithmic scale in decibels.[11–13]

Spectral-domain optical coherence tomography (SD-OCT) scans were done with Spectralis SD-OCT (Spectralis OCT, Version 6.3; Heidelberg Engineering, Heidelberg, Germany). Retinal nerve fiber layer was measured with a circular scan, 12° in diameter, centered on the BMO centroid (768 individual A-scans). The ONH was scanned with a radial scan protocol, consisting of 24 linear B-scans each consisting of 768 individual

Table 1. Demographic Data and Baseline Characteristics of the Study Cohort

Demographic and Baseline Parameter	Value
No. of eyes (subjects)	68 (108)
Age (mean ± SD, y)	69.0 (±9.1)
Sex (female/male) [%]	42/26 [61.8%/38.2%]
Race (AfA/HCA/AsA) [%]	10/46/12 [14.7%/67.6%/17.7%]
Laterality (right/left) [%]	53/55 [49%/51%]
Spherical equivalent (mean ± SD, D)	−0.7 (±1.8)
Axial length (mean ± SD, mm)	24.2 (±1.2)
MD (median and IQR, dB)	−5.9 (−12.6 to −3.6)
Global MRW (median and IQR, μm)	157.3 (122.1–191.2)
Global pRNFL (median and IQR, μm)	60.0 (52.0–73.0)
Normalized global MRW (median and IQR, μm)	157.7 (111.1–186.7)
Average change in global MRW after normalization (mean ± SD, μm)	1.7 (±17.9)
FoDi line angle (mean ± SD, degrees)	−7.8 (±4.2)

AfA, African American; AsA, Asian American; HCA, Hispanic-Caucasian American.

A-scans 6 mm in length in an emmetropic eye. Retinal nerve fiber layer segmentation, detection of Bruch membrane end-points to detect BMO and BMO-MRW calculation were performed automatically by the Glaucoma Module Premium Edition software (Heidelberg Engineering). However, the location of the BMO was corrected as needed by two experienced glaucoma specialists (FS and KNM). In some eyes with tilted ONHs, the device uses part of the Border Tissue of Elschnig (BTE) as the reference for calculating BMO-MRW. In such cases, the inner margin of the Bruch's membrane is located farther temporally and the BTE is actually a more appropriate reference for MRW estimation. In rare cases where the device detected the BMO erroneously, or where the measured BMO-MRW was obviously inaccurate, we manually corrected the location of the BMO. Images with a quality factor (Q) of 15 or higher were included in the study. All images were automatically aligned with the fovea-disc (FoDi) axis by the software.

To adjust the BMO-MRW for the BMO size, two methods were used: first, we normalized (scaled) the BMO-MRW thickness measurements based on the following formula according to average BMO circumference:

$$nBMO - MRW = \frac{BMO - MRW \times Circumferencee_{BMO}}{4.8} \quad (1)$$

where nBMO-MRW is the normalized BMO-MRW.

This method has been previously described by Patel and colleagues[14] in a normal database in which the average BMO circumference was calculated to be 4.8 mm. Second, we stratified the sample into small, average, and large discs based on the BMO area. As there are no widely accepted criteria for classifying the BMO area and because the BMO area had a normal distribution ($P = 0.733$, Wilk Shapiro test), we used the mean ± 1 SD as the boundaries for average disc size in our sample. Eyes with a BMO area more than the mean + 1 SD were considered to have large discs and those with BMO area lower than the mean − 1 SD were considered to have a small disc.

We also investigated the effect of BMO size and axial length on pRNFL measurement and SF relationships. To do this, we normalized pRNFL based on BMO using the same formula as used for nBMO-MRW:

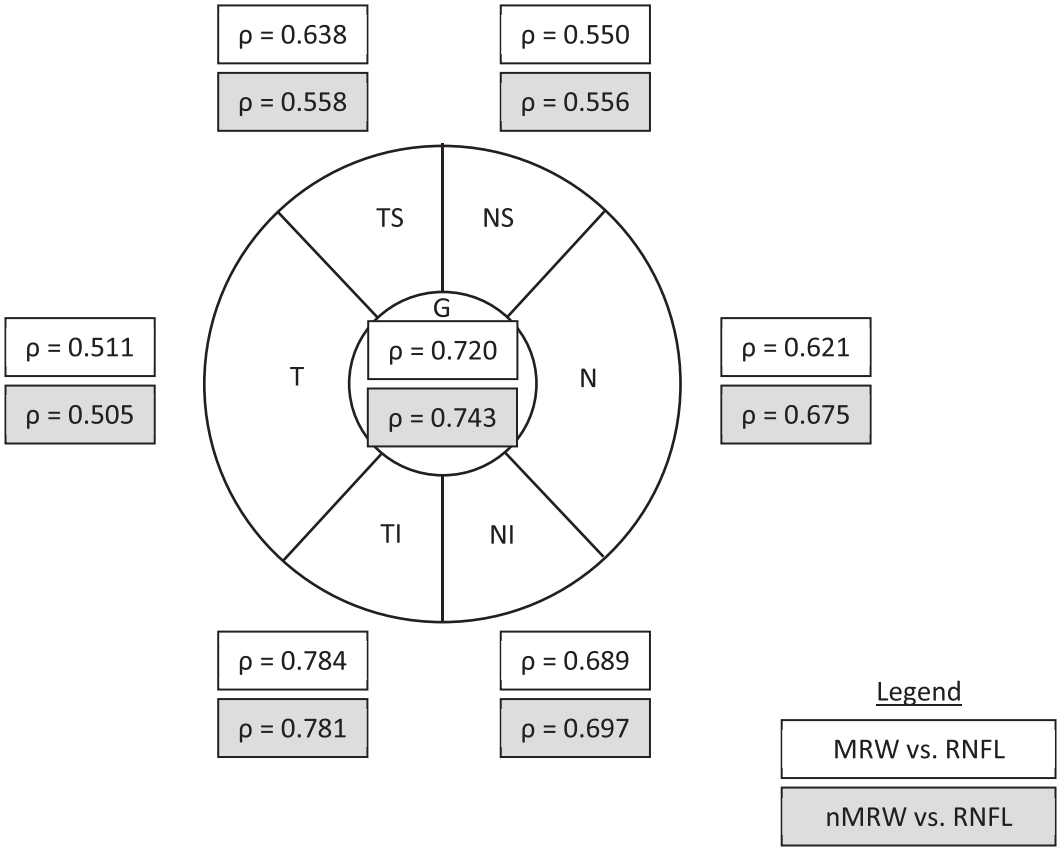

Figure 2. Spearman correlation coefficients between pRNFL and BMO-MRW before and after normalization based on BMO circumference.

$$n_{BMO}pRNFL = \frac{pRNFL \times Circumferencec_{BMO}}{4.8} \quad (2)$$

where n_{BMO}pRNFL is the normalized pRNFL based on BMO.

Furthermore, considering the possible effect of axial length on pRNFL measurement,[15] we used the following formula to normalize pRNFL measurement based on axial length in phakic subjects:

$$n_{AXL}pRNFL = \frac{pRNFL \times 24.46}{AXL} \quad (3)$$

where n_{AXL}pRNFL is the normalized pRNFL based on the patient's axial length (AXL) and 24.46 is the average AXL (in mm) assumed by the device database.

Statistical Analysis

Normal distribution of data was verified with Wilk-Shapiro test and review of Q–Q plots. Spearman correlation was used to estimate the strength of correlations between various structural and functional parameters. To address inclusion of the two eyes of the same patients, we used a within cluster resampling method (WCR) implemented in the software R.[16] A bootstrap method (with >1000 iteration) was used to compare the strength of correlation coefficients in a pairwise manner. We used the Benjamini–Hochberg method to address multiple comparisons.[17,18]

We have previously described our method for estimating the change point in SF plots.[19] Structure–function plots were constructed as bivariate plots with the VF sectoral AD on the X-axis and the corresponding BMO-MRW or pRNFL sectoral thickness (in μm) on the Y-axis. A broken stick model was fit to the SF data as follows:

$$Y = a \text{ if } X < C,\ Y = a + b(X - C) \text{ if } X \geq C \quad (4)$$

where a is the intercept in microns, an estimate of the measurement floor for BMO-MRW or pRNFL parameters; b is the slope for the change in BMO-MRW or pRNFL in microns for each decibel change in global MD or sectoral AD; and C is the global or sectoral VF threshold sensitivity at the point of change.

The model assumes that the BMO-MRW or pRNFL thicknesses reach their floor level at the change point, and that no change occurs beyond this point. Hence, a line with slope = 0 is fitted to the data below this point and a line with slope b is fitted to the data above the change point, C.

All statistical analyses were done with Stata version 14.0 (StataCorp LLC, College Station, TX, USA) and software R (Version 3.3.3).[20]

Results

One hundred eight eyes of 68 patients with open-angle glaucoma were included in the study. The mean age (±SD) was 69.0 (±9.1) years. The mean (±SD) axial length was 24.2 (±1.2) mm. The median (interquartile range [IQR]) MD was −5.9 dB (−12.6 to −3.6 dB) and it ranged between −25.7 and −0.1 dB. Table 1 summarizes demographic data and baseline clinical characteristics of the study sample.

Correlations Between Structural Parameters

The Spearman correlation coefficients between uncorrected BMO-MRW and pRNFL thickness varied between 0.51 and 0.78 (highest at temporal-inferior [TI] sector) and ranged between 0.50 and 0.78 after normalization for BMO circumference; however, the changes in the magnitude of correlations after normalization were not statistically significant ($P > 0.05$ for all the differences estimated with bootstrapping). Figure 2 summarizes the results.

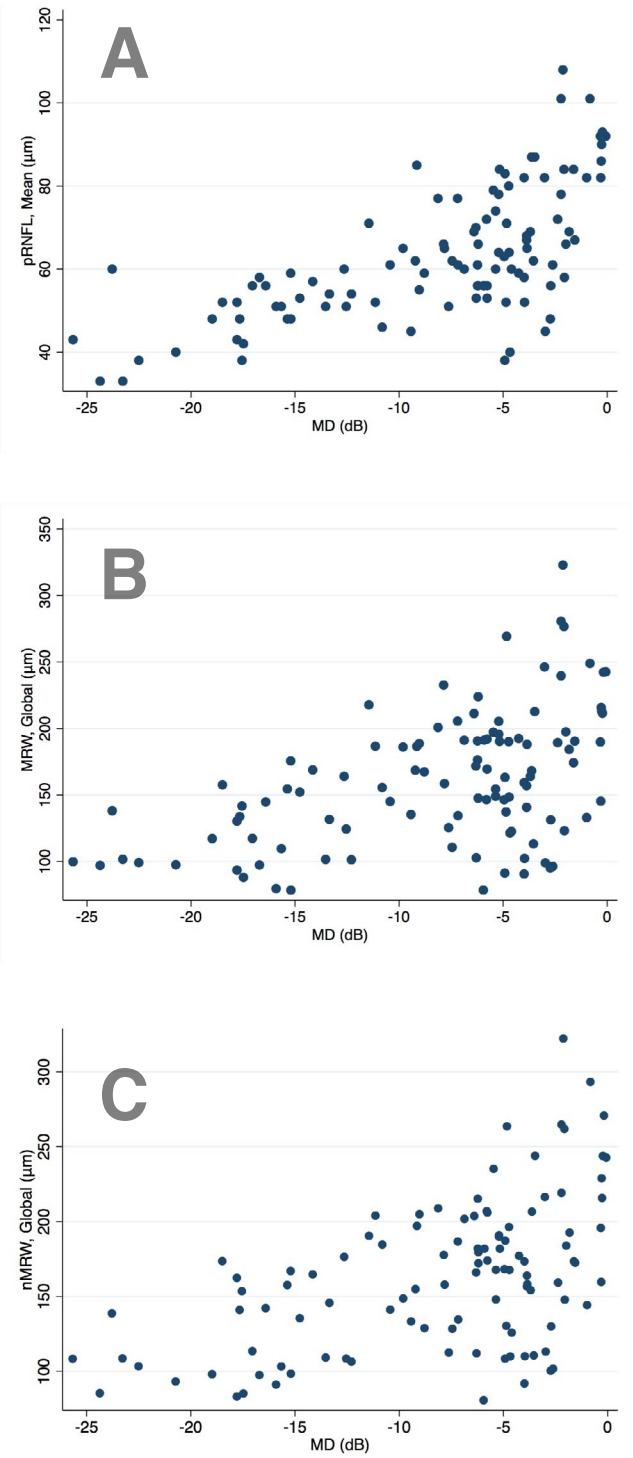

Figure 3. Scatter plots, demonstrating correlation of average pRNFL (**A**), global BMO-MRW (**B**) and normalized global BMO-MRW (**C**) with VF MD.

Correlations Between Structural and Functional Parameters

Scatterplots in Figure 3 show the relationship of average pRNFL thickness or global BMO-MRW with and without

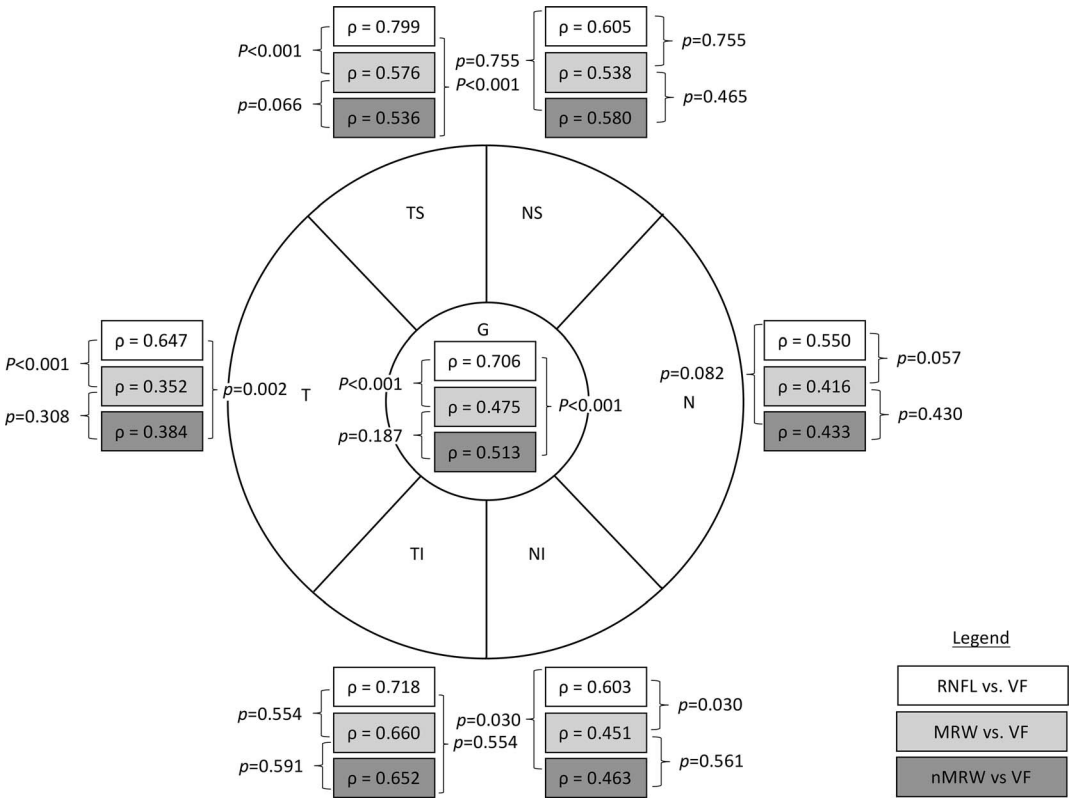

FIGURE 4. Spearman correlation coefficients between VF indices and various structural parameters. The comparison between correlation coefficients was performed with bootstrapping, with Benjamini–Hochberg correction.

normalization with VF MD. Also, scatter plots for sectoral structural parameters and corresponding AD are provided as Supplementary Material Figures S1–S7. The Spearman correlation coefficients between average and sectoral pRNFL thickness and global MD and AD in corresponding VF clusters, ranged from 0.55 (nasal sector) to 0.80 (temporal superior [TS] sector; Fig. 4). Using the same method, the Spearman correlation coefficient between average or sectoral BMO-MRW versus global or cluster-based VF AD ranged between 0.35 and 0.66 (lowest and highest at temporal and TI sectors, respectively). After normalizing BMO-MRW values based on BMO circumference (nBMO-MRW), these correlation coefficients changed to 0.38 to 0.65 (lowest and highest at temporal and TI sectors, respectively). The difference between Spearman correlations before and after normalizing BMO-MRW was not statistically significant ($P > 0.05$ for all comparisons estimated with bootstrapping with Benjamini–Hochberg correction; Fig. 4).

The Spearman coefficients for pRNFL versus VF correlation was larger than that for the BMO-MRW/VF in all the sectors and the difference was statistically significant for global measurement and temporal, TS, and nasal inferior (NI) sectors ($P < 0.03$, with Benjamini–Hochberg correction). The same results were found for corresponding pairs of pRNFL/VF coefficients and nBMO-MRW/VF ($P < 0.03$ for global and temporal, TS and NI sectors; Fig. 4). Normalization of pRNFL based on axial length or BMO circumference did not improve the SF relationship ($P > 0.05$ for all sectors and global measurements).

As described in the Methods section, we took into account the influence of the BMO size with two different approaches: (1) normalizing BMO-MRW measurements according to the BMO circumference, and (2) stratifying the measurements based on BMO area into small, average, and large discs and investigating its effect on the correlation between various structural variables and functional measures. The mean (±SD) BMO area was 1.89 (±0.39) mm^2; therefore, we considered a disc to be small when the BMO area was less than 1.50 mm^2 (17 eyes) and large when BMO area was greater than 2.29 mm^2 (18 eyes). Seventy-three eyes were considered to have an average BMO area (1.50–2.29 mm^2). In regression analyses with the VF MD or ADs as the dependent variable and the BMO-MRW, the BMO size (categorical variable) and their interaction as predictors, the BMO size category was not a significant predictor of VF MD or AD. The BMO area was inversely correlated with global BMO-MRW (Spearman's $\rho = -0.259$, $P = 0.033$). The scatter plot in Figure 5 shows changes in BMO-MRW and pRNFL as a function of BMO circumference. It can be observed that as the BMO area deviation from the average value increases, corrections to BMO-MRW and pRNFL become progressively larger.

On the broken stick models, the change point for global BMO-MRW or nBMO-MRW were displaced to the left compared with that of global pRNFL; however, as shown in Table 2, there was considerable overlap in the 95% confidence interval of the change points and the difference was not statistically significant. This pattern was not observed in any of the sectoral analyses. Normalization of BMO-MRW did not result in any observable shifts of the change point either globally or sectorally (Fig. 6). The model had a significant slope ($P < 0.0001$) after the change point for global measurements as well as sectoral ones. The change points on the broken stick SF models did not vary as a function of BMO area (data not shown). We compared the ratio of sectoral pRNFL, BMO-MRW, and nBMO-MRW thickness parameters divided by the corresponding average or global thickness. Significant differences were observed in the nasal and NI sectors between pRNFL and BMO-MRW

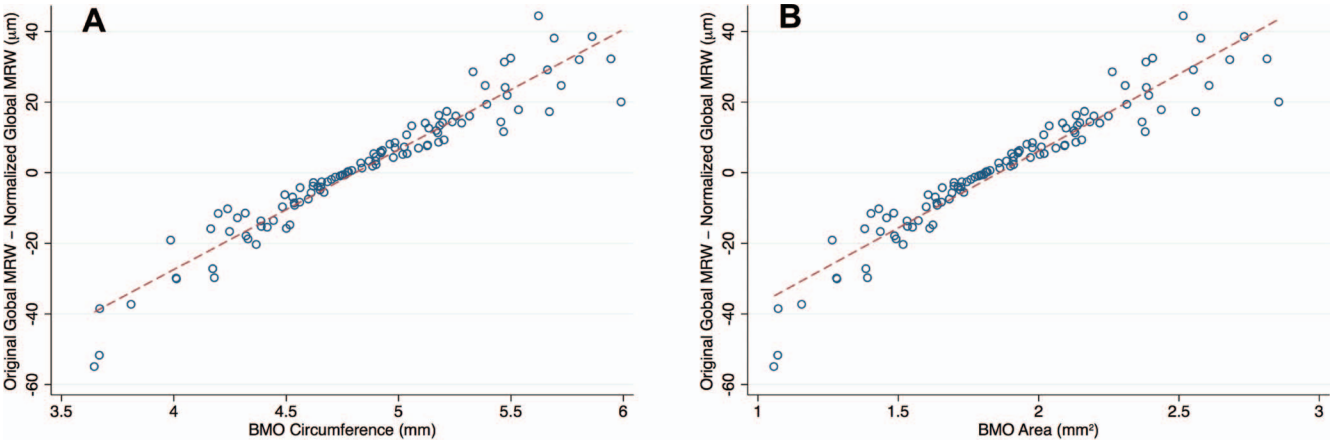

Figure 5. Scatter plots demonstrating changes in BMO-MRW thickness measurements as a function of BMO circumference (**A**) and BMO area (**B**).

parameters (lower ratio for pRNFL compared with BMO-MRW and nBMO-MRW; $P < 0.002$ for all comparisons).

Discussion

We herein report our findings on SF relationship in 108 eyes with perimetric glaucoma and a wide range of disease severity. Nonparametric correlations were explored between average/global and sectoral pRNFL thickness and BMO-MRW measurements, and both of these parameters with global MD or cluster-based VF ADs. To address correlation of the two eyes in bilaterally included cases, we used a WCR method and we addressed multiple comparisons with Benjamini–Hochberg correction. Overall, the SF relationships were similar between pRNFL, BMO-MRW, or nBMO-MRW and VF parameters. Compared with BMO-MRW, pRNFL thickness was more closely related to VF parameters globally and in all sectors, although this difference did not reach statistical significance in the nasal, NS, and TI sectors. We also explored the influence of the BMO area on BMO-MRW measures. We normalized the BMO-MRW estimates based on the BMO circumference as previously described by Patel and colleagues.[14] We also explored using the BMO circumference and axial length to normalize average pRNFL thickness. Analyses were repeated after data were stratified according to BMO area. We found that either approach did not significantly change SF relationship for BMO-MRW or pRNFL ($P > 0.05$ for all comparisons). The change point for global BMO-MRW extended to the left of that for the average pRNFL thickness denoting that global BMO-MRW might be useful for detection of structural change after average pRNFL has reached its measurement floor; however, this needs to be confirmed in larger scale, longitudinal studies as the difference was not found to be statistically significant.

Individual variability in the optic disc size, shape, and tilt, axial length, refractive error, cyclotorsion, and head position during image acquisition could affect structural measurements and influence SF relationships. Among these factors, optic disc size is an important confounding factor. We used BMO circumference as a surrogate for disc size but should point out that the two are not the same. We found a significant correlation between BMO-MRW and BMO area ($\rho = -0.26$, $P = 0.03$); this is in agreement with the findings by Tun et al.[21] in healthy subjects, and could be attributed to the fact that with larger BMO area, the retinal ganglion cell axons would be distributed along a larger circumference, and therefore would be relatively thinner. This is the rationale behind normalizing the BMO-MRW. To account for the influence of BMO area on SF relationships, we explored SF relationships after dividing BMO area into three groups or after normalizing BMO-MRW parameters based on BMO circumference. Neither of these methods consistently or significantly improved the correlation between various structural and functional parameters. This is in contrast to the findings of the study by Gmeiner and colleagues[5] who reported a better diagnostic performance of BMO-MRW in small discs with BMO area less than 1.84 mm^2. This difference could be due to different characteristics of the two cohorts and disease severity, as all of their cases were preperimetric or early glaucoma cases.[5] We used the average BMO circumference from Patel et al.[14] to normalize BMO-MRW measurements.

In the current study, pRNFL had an overall better correlation with VF compared with BMO-MRW and nBMO-MRW. There is no universal agreement regarding superiority of pRNFL or BMO-MRW as the optimal structural parameter for discrimination of glaucoma from healthy eyes. Some investigators such as Gmeiner et al.[5] and Gardiner and colleagues[6] reported similar performance whereas others did not.[2,4,22] This could be attributed to pRNFL thickness measurements being less influenced by the shape and anatomic variability of the optic disc along with more demanding segmentation of the BMO in addition to the factors mentioned above. However, as reported previously,[5] at various stages of the disease a subset of cases may be detected by one parameter and missed by the other and vice versa and therefore, the two parameters should be considered complementary.[5]

Normalization of pRNFL does not seem to be necessary. Huang and colleagues[15] demonstrated that optic disc size did not influence pRNFL thickness and the reported effect could be explained by differences in axial length and magnification error. The Spectralis device software addresses the magnification error by incorporating corneal curvature and power into its calculations.[23,24] Moreover, the focusing mechanism of the

Table 2. Change Points for Global Structural Parameters

Parameters	Change Point, dB	95% Confidence Interval, dB	
		Lower Bound	Upper Bound
pRNFL vs. MD	−10.2 ± 1.2	−12.6	−7.9
BMO-MRW vs. MD	−22.0 ± 5.2	−32.4	−11.7
nBMO-MRW vs. MD	−21.1 ± 4.7	−30.4	−11.8

MD was based on standard achromatic perimetry. Refer to the text for technical details in the Methods section.

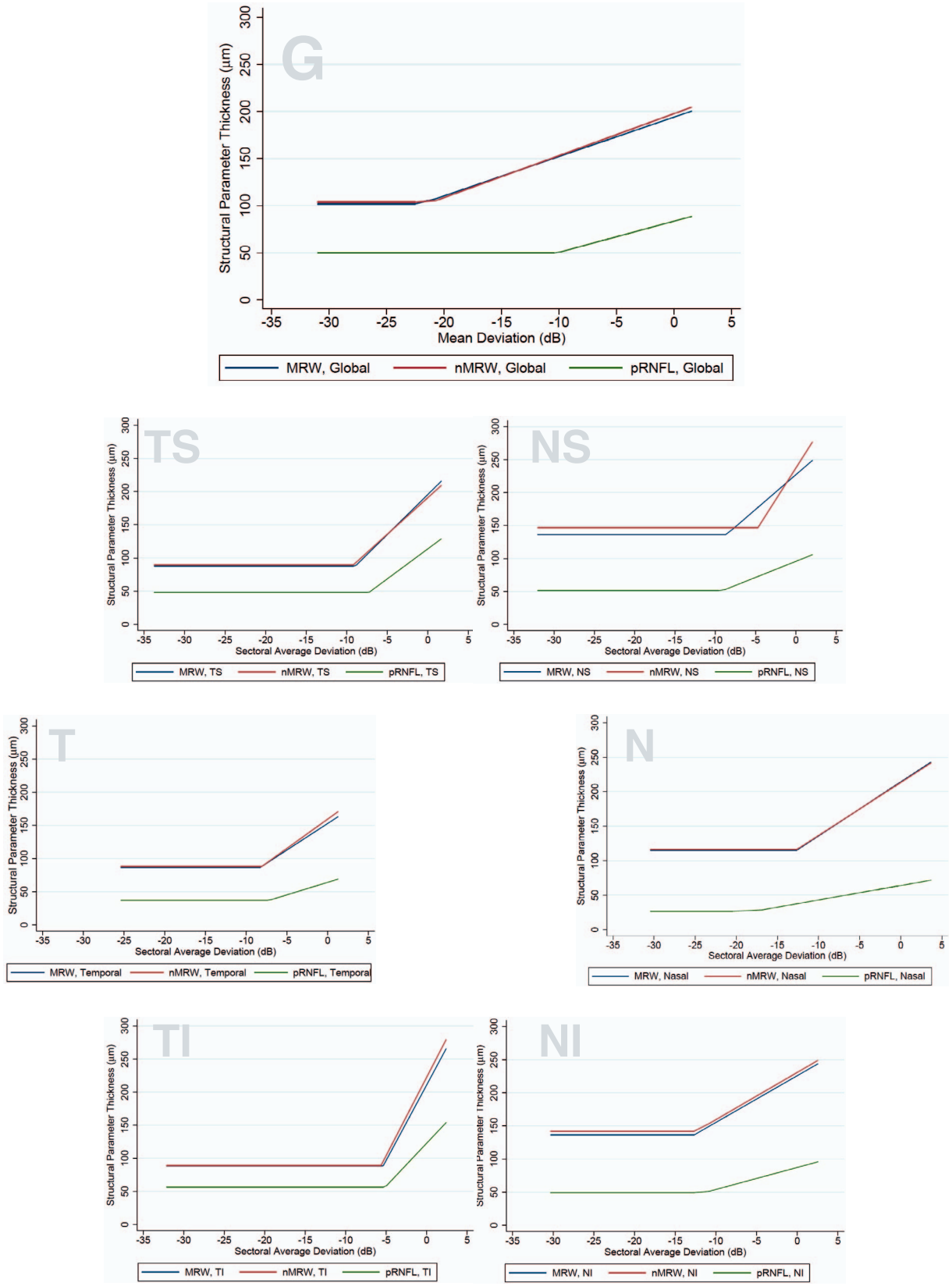

Figure 6. Change points of structural parameters based on VF defect severity for global (**A**) and sectoral (**B**) parameters.

device at least partially compensates for refractive error and reduces the magnification error.[25,26] We normalized pRNFL based on both BMO circumference and axial length and, as expected, there was no significant change in the results.

To investigate regional SF relationships, we used the maps by Garway-Heath et al.[9,10] There are several important issues to consider. Different types of glaucoma could vary with regard to severity, location, and extent of damage and this could affect the presentation of VF defects. Garway-Heath and colleagues suggested that based on the current body of knowledge, a similar map could be applied to all types of glaucoma.[27] The second issue is that, as mentioned by these investigators, their proposed mapping is valid in average eyes and it would be suboptimal in eyes with markedly shorter or longer axial length or those with an anomalous disc.[10] Most of our cases had near average axial lengths. Spectralis SD-OCT measurements are aligned along the FoDi axis, while the VFs are aligned on the geometric axis; however, this was not a major confounding factor in a previous study.[3] Given the large size of the sectors, it is unlikely that the results of this study were significantly influenced. Finally, it is worth noting that the derivation of the Garway-Heath[9,10] map is based on pRNFL defects that were detected clinically, and therefore, locations of defect were identified with respect to the clinical disc margin. A more appropriate way to define sectors and spatial relationships would be as a function of the BMO. This could be the topic of an interesting study in future.

There are several known factors that could affect proper automatic segmentation of ILM, including the location of blood vessels and the shape of the cup and disc.[28] In addition, Bruch's membrane may be absent in the area of peripapillary atrophy or might have decreased reflectivity in glaucoma and automated algorithms might no longer detect the BMO accurately.[29–31] All OCT images were reviewed by two of the authors (KNM and FS) to ensure proper segmentation of ILM and BMO, and hence, accurate BMO-MRW measurements. Almobarak and colleagues[30] compared the measurement error with automatic versus manual segmentation of ILM and BMO, and reported a median (IQR) difference in BMO-MRW measurement of 12.1 (10.1, 16.8) and 13.4 (10.6, 16.8) μm in healthy and glaucomatous subjects, respectively; neither was statistically significant.

One of the goals of our study was to compare the utility of pRNFL and BMO-MRW measures in more advanced glaucoma. Theoretically, if a structural measure reaches the measurement floor later than others (i.e., if it has a change point that occurs later) it could potentially be more useful for detecting disease progression in more advanced stages. To this aim, we compared the change point for various global and sectoral pRNFL and BMO-MRW parameters with the broken stick model.[13,32] Only the global BMO-MRW was found to have a change point to the left of that for the average pRNFL. We compared the ratio of sectoral RNFL, BMO-MRW, and nBMO-MRW thickness divided by the corresponding average or global thickness measurements to determine whether a larger residual thickness in nasal sectors could potentially explain the different change points for global BMO-MRW (and nBMO-MRW) thickness compared with the average RNFL thickness. We found a significantly higher ratio for MRW parameters in the nasal and NI sectors compared with pRNFL (denoting more prominent pRNFL loss as compared with BMO-MRW, $P < 0.002$ for all comparisons). These sectors are underrepresented in the Garway-Heath and colleagues' map as a smaller number of locations are measured in the corresponding VF clusters.[9,10] This finding needs to be confirmed in future studies before its utility can be fully realized in clinical practice. Normalization of BMO-MRW based on BMO area, did not significantly change the SF relationships. This could be attributed to the limited number of eyes with extreme BMO measurements in our study; it is also possible that larger discs could contain a higher proportion of nonneural tissues (blood vessels, glia, etc.) or that remodeling of neural tissues could slowly occur as glaucoma advances.

Our study had some limitations. Like many others studies, we used cross-sectional data. Optimally, correlation of longitudinal changes of various parameters over time could improve our understanding of the utility of such measures and would help clinicians choose the best parameter or combination of parameters to monitor progression of glaucoma. One caveat of studies such as ours is that the magnitude of the BMO-MRW correction depends on the distribution of the BMO area or circumference in the enrolled eyes. The small number of eyes with larger or smaller BMO area as defined in this study is a limitation that could have caused falsely negative results.

In conclusion, we found that BMO-MRW measures demonstrated somewhat weaker correlations with VF mean or average deviations as compared with pRNFL parameters in this group of eyes with a wide range of glaucoma severity. Structure–function relationships did not markedly change with normalization of BMO-MRW based on BMO circumference in this study. However, such corrections should be considered in eyes, in which the BMO size significantly deviates from the average values of the SD-OCT normative database.

Acknowledgments

Presented as a poster at the annual meeting of the Association for Research in Vision and Ophthalmology, May 3–7, 2015, Denver, Colorado, United States.

Supported by grants from the National Institutes of Health Mentored Patient-Oriented Research Career Development Award (K23EY022659; KNM; Bethesda, MD, USA) and an unrestricted Departmental Grant from Research to Prevent Blindness (New York, NY, USA). Also, technical and software support from Heidelberg Engineering (KNM; Heidelberg, Germany).

Disclosure: **N. Amini**, None; **R. Daneshvar**, None; **F. Sharifipour**, None; **P. Romero**, None; **S. Henry**, None; **J. Caprioli**, None; **K. Nouri-Mahdavi**, Heidelberg Engineering (F, R)

References

1. Gardiner SK, Boey PY, Yang H, Fortune B, Burgoyne CF, Demirel S. Structural measurements for monitoring change in glaucoma: comparing retinal nerve fiber layer thickness with minimum rim width and area. *Invest Ophthalmol Vis Sci*. 2015;56:6886–6891.
2. Chauhan BC, O'Leary N, Almobarak FA, et al. Enhanced detection of open-angle glaucoma with an anatomically accurate optical coherence tomography-derived neuroretinal rim parameter. *Ophthalmology*. 2013;120:535–543.
3. Danthurebandara VM, Sharpe GP, Hutchison DM, et al. Enhanced structure-function relationship in glaucoma with an anatomically and geometrically accurate neuroretinal rim measurement. *Invest Ophthalmol Vis Sci*. 2014;56:98–105.
4. Pollet-Villard F, Chiquet C, Romanet JP, Noel C, Aptel F. Structure-function relationships with spectral-domain optical coherence tomography retinal nerve fiber layer and optic nerve head measurements. *Invest Ophthalmol Vis Sci*. 2014; 55:2953–2962.
5. Gmeiner JM, Schrems WA, Mardin CY, Laemmer R, Kruse FE, Schrems-Hoesl LM. Comparison of Bruch's membrane opening minimum rim width and peripapillary retinal nerve fiber layer thickness in early glaucoma assessment. *Invest Ophthalmol Vis Sci*. 2016;57:OCT575–OCT584.
6. Gardiner SK, Ren R, Yang H, Fortune B, Burgoyne CF, Demirel S. A method to estimate the amount of neuroretinal rim tissue

in glaucoma: comparison with current methods for measuring rim area. *Am J Ophthalmol*. 2014;157:540–549.e2.

7. Hood DC. Relating retinal nerve fiber thickness to behavioral sensitivity in patients with glaucoma: application of a linear model. *J Opt Soc Am A Opt Image Sci Vis*. 2007;24:1426–1430.
8. Johnson CA, Sample PA, Cioffi GA, Liebmann JR, Weinreb RN. Structure and function evaluation (SAFE): I. criteria for glaucomatous visual field loss using standard automated perimetry (SAP) and short wavelength automated perimetry (SWAP). *Am J Ophthalmol*. 2002;134:177–185.
9. Garway-Heath DF, Holder GE, Fitzke FW, Hitchings RA. Relationship between electrophysiological, psychophysical, and anatomical measurements in glaucoma. *Invest Ophthalmol Vis Sci*. 2002;43:2213–2220.
10. Garway-Heath DF, Poinoosawmy D, Fitzke FW, Hitchings RA. Mapping the visual field to the optic disc in normal tension glaucoma eyes. *Ophthalmology*. 2000;107:1809–1815.
11. Hood DC, Greenstein VC, Odel JG, et al. Visual field defects and multifocal visual evoked potentials: evidence of a linear relationship. *Arch Ophthalmol*. 2002;120:1672–1681.
12. Hood DC, Zhang X. Multifocal ERG and VEP responses and visual fields: comparing disease-related changes. *Doc Ophthalmol*. 2000;100:115–137.
13. Hood DC, Kardon RH. A framework for comparing structural and functional measures of glaucomatous damage. *Prog Retin Eye Res*. 2007;26:688–710.
14. Patel NB, Sullivan-Mee M, Harwerth RS. The relationship between retinal nerve fiber layer thickness and optic nerve head neuroretinal rim tissue in glaucoma. *Invest Ophthalmol Vis Sci*. 2014;55:6802–6816.
15. Huang D, Chopra V, Lu AT, et al. Does optic nerve head size variation affect circumpapillary retinal nerve fiber layer thickness measurement by optical coherence tomography? *Invest Ophthalmol Vis Sci*. 2012;53:4990–4997.
16. Lorenz DJ, Datta S, Harkema SJ. Marginal association measures for clustered data. *Stat Med*. 2011;30:3181–3191.
17. Mangiafico SS. An R Companion for the Handbook of Biological Statistics. Version 1.3.0. 2013. Available at: http://rcompanion.org/rcompanion/f_01.html. Accessed July 12, 2017.
18. Hochberg Y, Benjamini Y. More powerful procedures for multiple significance testing. *Stat Med*. 1990;9:811–818.
19. Nilforushan N, Nassiri N, Moghimi S, et al. Structure-function relationships between spectral-domain OCT and standard achromatic perimetry. *Invest Ophthalmol Vis Sci*. 2012;53:2740–2748.
20. R Core Team (2017). R: A language and environment for statistical computing. R Foundation for Statistical Computing, Vienna, Austria. Available at: https://www.R-project.org/. Accessed July 12, 2017.
21. Tun TA, Sun CH, Baskaran M, et al. Determinants of optical coherence tomography-derived minimum neuroretinal rim width in a normal Chinese population. *Invest Ophthalmol Vis Sci*. 2015;56:3337–3344.
22. Muth DR, Hirneiss CW. Structure-function relationship between Bruch's membrane opening-based optic nerve head parameters and visual field defects in glaucoma. *Invest Ophthalmol Vis Sci*. 2015;56:3320–3328.
23. Amini N, Miraftabi A, Henry S, et al. The relationship of the clinical disc margin and Bruch's membrane opening in normal and glaucoma subjects. *Invest Ophthalmol Vis Sci*. 2016;57:1468–1475.
24. Ctori I, Gruppetta S, Huntjens B. The effects of ocular magnification on Spectralis spectral domain optical coherence tomography scan length. *Graefes Arch Clin Exp Ophthalmol*. 2015;253:733–738.
25. Nowroozizadeh S, Cirineo N, Amini N, et al. Influence of correction of ocular magnification on spectral-domain OCT retinal nerve fiber layer measurement variability and performance. *Invest Ophthalmol Vis Sci*. 2014;55:3439–3446.
26. Sanchez-Cano A, Baraibar B, Pablo LE, Honrubia FM. Magnification characteristics of the Optical Coherence Tomograph STRATUS OCT 3000. *Ophthalmic Physiol Opt*. 2008;28:21–28.
27. Spaeth GL. Mapping the visual field. *Ophthalmology*. 2001;108:1714.
28. Miri MS, Robles VA, Abramoff MD, Kwon YH, Garvin MK. Incorporation of gradient vector flow field in a multimodal graph-theoretic approach for segmenting the internal limiting membrane from glaucomatous optic nerve head-centered SD-OCT volumes. *Comput Med Imaging Graph*. 2017;55:87–94.
29. Akagi T, Iida Y, Nakanishi H, et al. Microvascular density in glaucomatous eyes with hemifield visual field defects: an optical coherence tomography angiography study. *Am J Ophthalmol*. 2016;168:237–249.
30. Almobarak FA, O'Leary N, Reis AS, et al. Automated segmentation of optic nerve head structures with optical coherence tomography. *Invest Ophthalmol Vis Sci*. 2014;55:1161–1168.
31. Hwang YH, Kim MK, Ahn SI. Consistency of Bruch membrane opening detection as determined by optical coherence tomography. *J Glaucoma*. 2016;25:873–878.
32. Miraftabi A, Amini N, Morales E, et al. Macular SD-OCT outcome measures: comparison of local structure-function relationships and dynamic range. *Invest Ophthalmol Vis Sci*. 2016;57:4815–4823.

Investigative Ophthalmology & Visual Science